Recombination through amphoteric states at the amorphous/crystalline silicon interface: modelling and experiment

Sara Olibet, Evelyne Vallat-Sauvain, Christophe Ballif, Luc Fesquet

Institute of Microtechnology (IMT), University of Neuchâtel, Breguet 2, CH-2000 Neuchâtel, Switzerland.

Abstract

The performance of high-efficient crystalline silicon (c-Si) based solar cells is, besides bulk recombination, limited by the recombination losses on both c-Si surfaces. Dangling bonds at the c-Si surface are the defects governing interface recombination irrespective of the overlaying passivation layer (i.e. SiO_2, Si_xN_y, a-Si:H). Dangling bonds are also the predominant defects governing recombination in bulk hydrogenated amorphous silicon (a-Si:H). Considering the amphoteric nature of these defects (i.e. different charge states when singly, doubly or not occupied), a closed-form expression exists for recombination in bulk a-Si:H. The application of this dangling bond recombination formalism to c-Si surface dangling bond recombination in the otherwise classical approach allows us to reproduce the measured injection-level dependence of the a-Si:H/c-Si interface recombination. Thus we can quantify the respective contribution of the two fundamental mechanisms of surface passivation: the interface defect density and the image charge density in the c-Si induced by the charged defects in the a-Si:H passivation layer. Our experimental data contains a large variety of configurations of c-Si/a-Si:H layers. The flat c-Si wafers are of different doping level and doping type (including intrinsic) and the average charge state of the amphoteric recombination centers in the passivating intrinsic a-Si:H layers is varied by microdoping or by capping the passivation layers with doped layers. The good interface passivation properties of a-Si:H layers are exploited in heterojunction solar cells: By a straight-forward development resulting from our passivation studies, we are achieving so far a best V_{OC} of 705mV (with 17.5% efficiency and a *FF* of 78%) and a best device efficiency of 19% (with a V_{OC} of 680mV and a fill factor (*FF*) of 82%) on flat 1Ωcm *n*-type c-Si. For example these trade-offs between V_{OC} and *FF* can partly be linked to the injection-level dependent interface recombination as the V_{OC} corresponds to rather high injection-levels ($\sim 5\cdot 10^{15}cm^{-3}$), whereas the maximum power point (*MPP*) corresponds to medium injection-levels ($\sim 5\cdot 10^{14}cm^{-3}$).

1. Introduction

One of the major concerns for crystalline silicon (c-Si) solar cells is the unwanted recombination of free charge carriers. Photogenerated charge carriers that either recombine in the semiconductors bulk or at its surface reduce the solar cells performances. The dominant recombination mechanism of free charge carriers in high bulk lifetime semiconductors is thus the recombination via electrically active centres at its surface. By an appropriate surface passivation – overall free carriers lifetime maximization by rendering c-Si surface dangling bonds electrically and chemically passive – the effective diffusion lengths of the photogenerated charge carriers reach several times the c-Si wafer thickness.

Usual surface passivation schemes use silicon dioxide (SiO_2) [1] or silicon nitride (SiN_x) [2]. An alternative to these is hydrogenated amorphous silicon (a-Si:H) grown at low temperature (around 200°C). On the one hand a-Si:H passivates c-Si by hydrogen termination of interface dangling bonds. If, on the other hand, the passivating a-Si:H layer is charged, the presence of one carrier type in the c-Si near the interface is reduced by field effect, i.e. recombination is hindered by the lack of one recombination partner. When passivating c-Si with a-Si:H, we can thus tune the respective contribution of these two different mechanisms governing interface recombination. We find their respective influence by modelling the injection-level dependence of this interface recombination through amphoteric states with a simple existing a-Si:H bulk recombination formalism in the otherwise classical surface recombination approach. In this paper, we show that improving interface passivation and understanding the related mechanisms by fitting experimental data with our model, speeds up the achievement of high performance a-Si:H/c-Si heterojunction solar cells.

2. Modelling interface recombination

The recombination efficiency of interface defects is governed by their nature, whereas the recombination rate depends strongly on the surface carrier densities which vary with the illumination-level.

2.1 Crystalline silicon surface recombination

The first step to model interface recombination is the determination of the surface carrier densities $n_S = n_d \cdot \exp(q\Psi_S/kT)$ and $p_S = p_d \cdot \exp(-q\Psi_S/kT)$ [cm^{-3}] under surface band bending conditions ($\Psi_S \neq 0$) inducing a surface space charge region and leading therefore to non-equal excess surface carrier densities, i.e. $\Delta n_S \neq \Delta p_S$. Figure 1 illustrates the situation. The carrier densities at the edge of the surface space charge region n_d and p_d are equal to the carrier densities in the bulk, $n_d = n = n_0 + \Delta n$ and $p_d = p = p_0 + \Delta p$, where

the excess carrier densities are equal, i.e. $\Delta n = \Delta p$. n_0 and p_0 are the bulk equilibrium carrier densities that are given by the c-Si doping. The surface potential Ψ_S can be found by solving the non-linear equation for the induced c-Si surface space charge density Q_{Si} [cm^{-2}]:

$$Q_{Si} = \pm\sqrt{\frac{2kTn_i\varepsilon_0\varepsilon_{Si}}{q^2}[e^{q(\phi_p-\psi_S)/kT} - e^{q\phi_p/kT} + e^{q(\psi_S-\phi_n)/kT} - e^{-q\phi_n/kT} + \frac{q\psi_S(p_0+n_0)}{kTn_i}]}\,, \quad (1)$$

where $\phi_n = -kT/q\cdot\ln(n/n_i)$ and $\phi_p = +kT/q\cdot\ln(p/n_i)$, the quasi-Fermi levels of electrons and holes, vary with the excess carrier densities and Ψ_S is therefore illumination-level dependent too. The other parameters have their usual meaning [3].

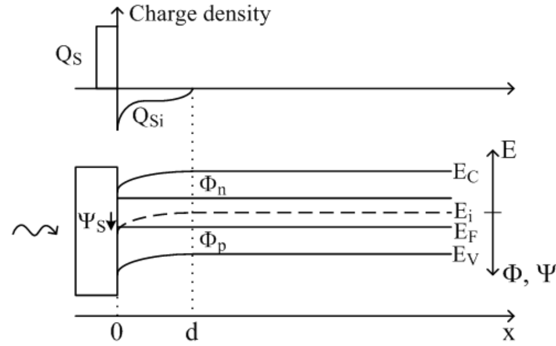

Figure 1 Band diagram and charge distribution of a-Si:H passivating p-type doped c-Si under illumination.

Once Ψ_S is found, n_S and p_S can be calculated. Up to this point, this is the standard surface recombination calculation for c-Si passivation with a dielectric [4].

2.2 a-Si:H bulk recombination

The second step towards an interface recombination model is the choice of an interface recombination function according to the interface defects nature. By passivating crystalline silicon with amorphous silicon, we make the assumption that there are only intrinsic silicon dangling bonds at the interface. Also in bulk a-Si:H recombination occurs through intrinsic silicon dangling bonds. Dangling bonds are amphoteric recombination centres – this means that the Si_3 site can have three charge states: unoccupied, occupied by 1 electron or by 2 electrons. Successive capture events at these differently charged dangling bonds lead to recombination. Figure 2 illustrates the two possible recombination paths that co-exist. This recombination mechanism is an extension of the usual Shockley-Read-Hall recombination which assumes only two possible states of the recombination centres (unoccupied or occupied by 1 electron).

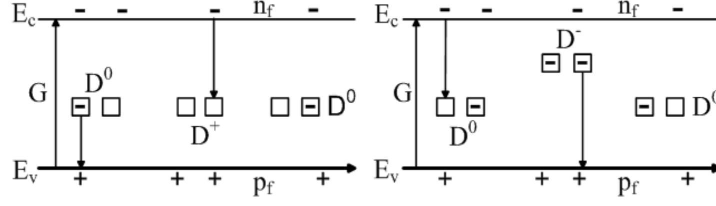

Figure 2 Successive capture events leading to free electron-hole pair recombination through D_0. Two paths co-exist.

A closed form expression for this bulk a-Si:H recombination through amphoteric defects was developped by *Hubin et al.* in 1992 [5]:

$$R_{DB} = \frac{n_f \sigma_n^0 + p_f \sigma_p^0}{\frac{p_f}{n_f}\frac{\sigma_p^0}{\sigma_n^+} + 1 + \frac{n_f}{p_f}\frac{\sigma_n^0}{\sigma_p^-}} v_{th} N_{DB} \;\; [\mathrm{cm}^{-3}\mathrm{s}^{-1}]. \tag{2}$$

Besides the bulk dangling bond density N_{DB} and the free carrier densities n_f and p_f this recombination rate depends on the capture cross-sections σ that are different for the carrier type and the charge state.

2.3 Amphoteric a-Si:H/c-Si interface recombination

To model interface recombination through amphoteric recombination centres, we chose thus the two-dimensional version of the bulk amorphous silicon recombination rate by simply replacing the bulk dangling bond density N_{DB} [cm^{-3}] by a surface dangling bond density N_S [cm^{-2}]:

$$U_S = U_{DB} = \frac{n_S \sigma_n^0 + p_S \sigma_p^0}{\frac{p_S}{n_S}\frac{\sigma_p^0}{\sigma_n^+} + 1 + \frac{n_S}{p_S}\frac{\sigma_n^0}{\sigma_p^-}} v_{th} N_S \;\; [\mathrm{cm}^{-2}\mathrm{s}^{-1}], \tag{3}$$

where n_S and p_S are calculated as described in Sub-section 2.1. The quantification of interface recombination is made by defining the effective surface recombination velocity S_{eff} at the edge of the space-charge region where the excess carrier densities *ECD* are equal, i.e. $\Delta n_d = \Delta p_d = \Delta n = \Delta p = ECD$ [4]:

$$S_{eff} \equiv U_S / \Delta n \;\; [\mathrm{cm/s}]. \tag{4}$$

This injection-level dependent surface recombination velocity is experimentally accessible. By fitting experimental $S_{eff}(ECD)$-curves with our model we can thus quantify the two microscopic mechanisms governing interface recombination: the interface defect density N_S [cm^{-2}] and the charge density induced in the c-Si Q_{Si} [cm^{-2}].

3. Experimental

3.1 a-Si:H layer growth on c-Si

Double-side polished float zone monocrystalline silicon wafers are sequentially passivated on both sides by intrinsic a-Si:H layers. Intrinsic or lightly doped c-Si wafers of both *n* and *p* doping type are chosen for the passivation studies to ensure a maximum sensibility to surface recombination by high bulk lifetimes τ_b over the whole injection-level range (τ_b = 10ms assumed). To modify the average state of charge of the dangling bond defects in the passivating a-Si:H layers, they are lightly doped or covered by doped layers.

Hydrogenated amorphous silicon layers are grown by VHF-PECVD (very-high frequency plasma enhanced chemical vapour deposition) at an excitation frequency of 70MHz and a deposition temperature of 180°C in a single chamber plasma reactor. The passivating intrinsic (*i*) and microdoped (µdop) a-Si:H layers are grown from silane (SiH_4) and hydrogen (H_2) as source gases with a hydrogen dilution of 2.5 ($H_{dil} = [H_2]/[SiH_4]$), whereas a few ppm of trimethylborane (TMB) or phosphine (PH_3) is added for *p*-type, resp. *n*-type microdoping. Microdoping aims to modify the average state of charge of silicon dangling bonds without increasing their density – as is done by doping. Conditions similar to those applied for a-Si:H solar cell fabrication are used to grow the (more defective) doped layers from a mixture of SiH_4, H_2 and TMB for *p*-type, resp. PH_3 for *n*-type doping. After growth a-Si:H layers are thermally annealed at the deposition temperature (180°C).

3.2 Lifetime measurements

The quantity experimentally accessible by measuring surface passivation of high quality monocrystalline silicon wafers passivated by a-Si:H, is the effective lifetime τ_{eff} as function of the excess carrier densities (*ECD*). The Sinton Lifetime Tester [6] measures inductively photoconductance vs time during (quasi-steady-state QSS) or after (transient) a decaying light pulse. The effective surface recombination velocity S_{eff} of symmetrically passivated c-Si wafers is related to the injection-level dependent τ_{eff} by:

$$S_{eff} = (1/\tau_{eff} - 1/\tau_b) \cdot W/2\,, \tag{5}$$

where W is the wafer thickness. As an example, Figure 3(a) shows the passivation performance of a *n*-type microdoped a-Si:H layer on a *n*-type c-Si wafer with a resistivity of 28Ωcm and 111 crystal orientation. The maximal measured τ_{eff} of 3 ms corresponds, on this 255µm thick wafer, to a S_{eff} as low as 2cm/s.

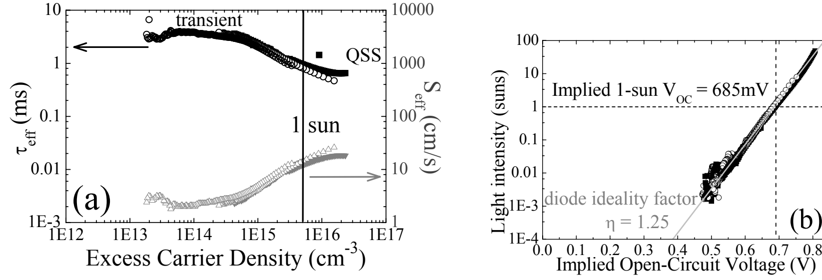

Figure 3 (a) Example of injection-level dependent τ_{eff} as measured by the photoconductance decay technique with the Sinton lifetime tester in the transient as well as in the QSS mode. S_{eff} as calculated by Eq. (5) is roughly inversely proportionnal to W/τ_{eff}. (b) Prediction of the illumination-level dependent V_{OC} resulting from this $\tau_{eff}(ECD)$-curve.

The open-circuit voltage V_{OC} of a final device is given by the splitting of the quasi-Fermi levels:

$$V_{OC} = \phi_p - \phi_n = kT/q \cdot \ln(np/n_i^2)\,. \qquad (6)$$

We cane thus acquire, together with the lifetime, a prediction of the illumination-level dependent V_{OC} of a solar cell with this $\tau_{eff}(ECD)$-curve as shown in Figure 3(b). On the $\tau_{eff}(ECD)$-curve in Figure 3(a), ECD corresponding to the 1-sun illumination-level is indicated.

3.3 Silicon heterojunction solar cells

By growing asymmetrical stacks of thin intrinsic (about 5nm) plus doped a-Si:H layers on c-Si, we obtain a silicon heterojunction solar cell precursor. Due to this asymmetrical structure, the measured $\tau_{eff}(ECD)$-curve results from a mixture of both c-Si sides passivation.

Finally, our silicon heterojunction solar cells are prepared by contacting these asymmetrical stacks onto both sides by transparent conductive oxides and back metallization – e.g. on *n*-type doped c-Si ITO / *p*/*i* a-Si:H / *n* c-Si / *i*/*n* a-Si:H / ITO / Al or Ag – and structuring these into small 5x5mm^2 sized individual cells. The interface recombination properties of these completed solar cells are studied by the Sinton Suns-V_{OC} measurement set-up [7] that measures directly the open-circuit voltage as a function of the illumination-level. By inverting Eq. (6), we find again the injection-level dependent τ_{eff}. In addition, a pseudo light *IV*-curve can be calculated, that is an *IV*-curve without series resistance as no current is extracted from the cell. Finally, the true electrical characteristics of the solar cell are measured in a standard way by varying the applied voltage *V* and thus extracting current *I* under 1-sun

illumination. The absolute value of current is obtained from external quantum efficiency measurements.

4. Fitting to experimental data

Our aim is to fit experimental data with our model using the two single model variables N_S and Q_{Si} distinguishing the two microscopic mechanisms of interface recombination. For that, we fix the capture cross-sections in Eq. (3) to the values allowing the best fit to the complete set of intrinsic a-Si:H layers passivating differently doped c-Si. The values that allow a proper fit of all curves are $\sigma_n^0/\sigma_p^0 = 1/20$ and $\sigma_n^+/\sigma_n^0 = \sigma_p^-/\sigma_p^0 = 500$.

Thus, as a first example of fitting to experimental data, Figures 4(a),(b) show the passivation properties of 5nm and 40nm thick *i* a-Si:H layers grown symmetrically on different c-Si wafers. The resulting $S_{eff}(ECD)$-curves are well reproduced by our model with reasonable values for the two fit parameters N_S and Q_{Si}.

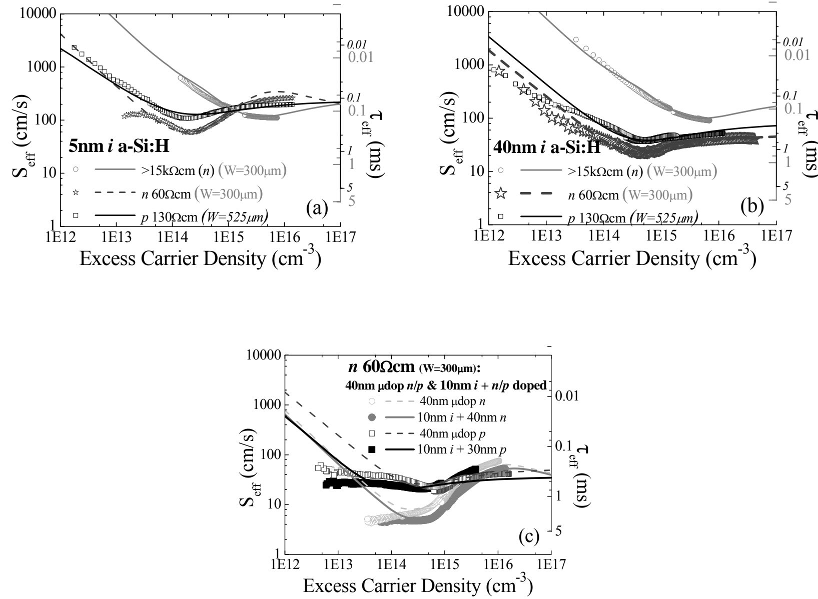

Figure 4 Measured (symbols) and fitted (lines) $S_{eff}(ECD)$-curves of c-Si passivated symmetrically with a-Si:H layers. (a), (b) 5nm resp. 40nm *i* a-Si:H passivating three different c-Si wafers of thickness W. There are two indicative τ_{eff}-scales on the right hand, the one in italic corresponding to the thicker *p*-type wafer. (c) Passivation of the same c-Si wafer with µdop and stacks of intrinsic plus doped a-Si:H layers of both doping types.

Figure 4(c) shows that, as expected, changing the dangling bond charge state in the *i* a-Si:H layer by microdoping or by fixing its outer potential by the growth of a doped a-Si:H layer results in similar $S_{eff}(ECD)$-curves. Again, the best fits to experimental data yield reasonable agreements for the two only model fit parameters, e.g. the sign of Q_{Si} is the opposite of the average dangling bond charge state in the passivating layers. The low injection-level discrepancies are due to the simplifying assumptions made on the a-Si:H density of states to find Eq. (2). Whereas lower minimal S_{eff} values are reached by field effect when c-Si is passivated by *n* µdop layers and *i*/*n* double-layer stacks, the layers including *p*-type doping are not able to achieve efficient supplementary field effect passivation as can be noticed by comparing the star symbols in Figure 4(b) to the curves in Figure 4(c) – this observation is verified to be independent of the c-Si doping type (not shown here).

5. Accelerated silicon heterojunction solar cell development

In this article, we aim to have a look at the potential of speeding up silicon heterojunction solar cell development by injection-level dependent lifetime measurements and modelling of interface recombination in symmetrically a-Si:H passivated c-Si wafers.

5.1 Good passivation leads to high open-circuit voltages

To study the final solar cells V_{OC} prediction capabilities of injection-level dependent lifetime measurements on silicon heterojunction solar cell precursors, we first examine the case of our highest-V_{OC} flat solar cell as shown in Figure 5. Indeed, the V_{OC} of 705mV of the final solar cell is excellently predicted by lifetime measurements on the non-contacted solar cell precursor. Because of the asymmetrical passivation structure, Figure 5(a) shows mainly $\tau_{eff}(ECD)$-curves as measured, indicating with the right hand axis the corresponding S^*_{eff} values. In this case an average of front and back surface passivation, i.e. $S^*_{eff} = (S_{front} + S_{back})/2$ $(= (1/\tau_{eff} - 1/\tau_b)\cdot W/2)$. Furthermore, from Figure 5(a) we recognize that the passivation performance of the asymmetrical stacks of intrinsic plus doped a-Si:H layers remains unchanged after further contact deposition, as the $\tau_{eff}(ECD)$-curves overlap. Additionally Figure 5(b) tells us that the real fill factor (*FF*) is more than 4% lower than the one without series resistance even though recombination of carriers passing through the heterojunction can not be extruded – i.e. 78% instead of 82.5%. These observations hold also for *p*-type c-Si.

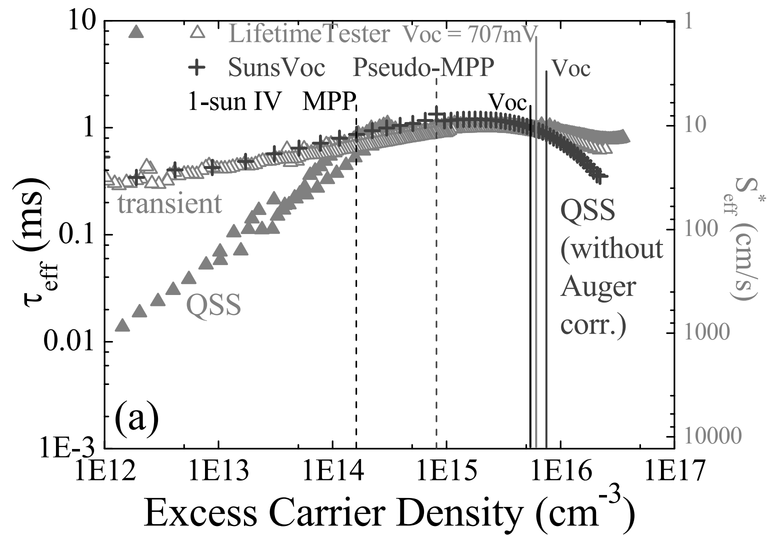

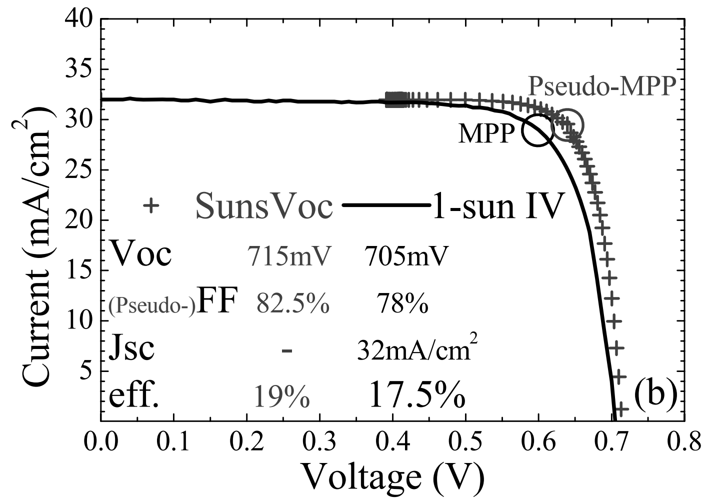

Figure 5 Silicon heterojunction solar cell based on 250µm thick 1Ωcm *n*-type c-Si. (a) $\tau_{eff}(ECD)$-curves measured on the solar cell precursor (gray triangle symbols) as well as after further contact deposition (dark gray plus symbols). *ECD* corresponding to V_{OC} and *MPP* (maximum power point) is indicated for the different measurements. (b) Pseudo light-*IV* curve (dark gray plus symbols) compared to final 1-sun *IV*-curve (black line).

5.2 From symmetrical passivation with single a-Si:H layers to final device performance

We now consider the complete development from symmetrical passivation with single a-Si:H layers to final solar cell performance on another wafer type – *n*-type, 28Ωcm, flat, crystal orientation 111 –, as shown in Figure 6. Passivation with intrinsic and *n*-type µdop single layers is good, that means it yields high lifetimes, i.e. low surface recombination velocities as shown in Figure 6(a) (symbols). Again, the measured injection-level dependent interface recombination can be well reproduced by our model (lines). A V_{OC} of 670mV with double-side intrinsic, resp. 685mV with double-side *n* µdop passivation could be reached. The silicon heterojunction solar cell precursor fabricated by growing asymmetrical stacks of intrinsic plus doped layers shows as well low interface recombination (grey triangle symbols) and further metallic contact deposition preserves this (dark grey plus symbols) as shows Figure 6(b). The calculated pseudo *IV*-curve yields a rather low *pseudo-FF* of 77%, due to a larger diode ideality factor η at medium illumination-levels (corresponding to *MPP*) of this solar cell compared to the highest-V_{OC} cell discussed in Sub-section 5.1 – η = 2.1 instead of η = 1.25. This higher η results from a less favourable injection-level dependence of τ_{eff} in Figure 6(b) compared to Figure 5(a), visualized by a lower ratio $\tau_{eff}(V_{OC})/\tau_{eff}(MPP)$. But the symmetrical passivation of the same c-Si wafer with *n* µdop layers yields also a favourable η = 1.25 as shown in Figure 3(b). Thus again as already remarked in Section 4, the *i*/*p*-stack is unable to raise carrier lifetimes remarkably at injection-levels corresponding to the *MPP*.

However, only the final 1-sun *IV*-curve measurement shows that this cell has a serious collection problem not mainly related to a high series resistance as shows the inset in Figure 6(c). The S-shaped curve is attributed to excess carrier recombination in the *i*-layer and at the *i*-*p* interface, when minority carriers are allowed to go through the front interface. When no current is flowing through the cell at 1-sun illumination, we have the same conditions in both measurements – 1-sun *IV* and Suns-V_{OC} – and thus the two curves cross at 1-sun V_{OC}. Nevertheless the improvement and deeper understanding of symmetrically single a-Si:H layer passivation accelerates appreciably the achievement of good solar cell performances, because the S-shaped *IV*-curves can be relatively easily eliminated by fine-tuning the a-Si:H layer deposition parameters. By tuning the injection-level dependence of interface recombination such as to approach ideal diode behaviour η = 1 and thus raising *FF*, we succeeded in fabricating a 19% efficient cell with *FF* = 82% - regardless of the loss in V_{OC} (here V_{OC} = 680mV) correlated with an improved diode ideality factor, as evaluated from lifetime and Suns-V_{OC} measurements.

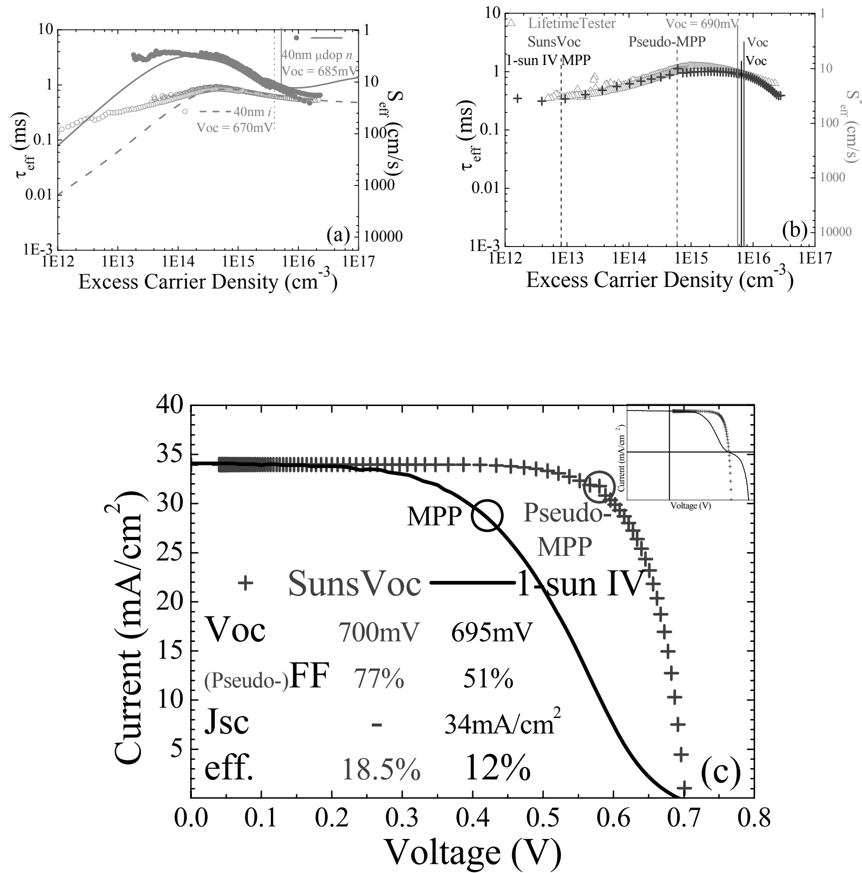

Figure 6 Silicon heterojunction solar cell development from symmetrical single a-Si:H layer passivation to final solar cell performances on a flat *n*-type 28Ωcm c-Si wafer with 111 crystal orientation: (a),(b) $\tau_{eff}(ECD)$-curves from photoconductance and Suns-V_{OC} measurements, (c) pseuso light-*IV* and 1-sun *IV*-curves.

6. Conclusions

We present a new simple model for crystalline silicon (c-Si) surface recombination through silicon dangling bonds that is based on their amphoteric nature. Except for some low injection-level discrepancies, which are attributed to the role of the bandtails, our model yields a good reproduction of the experimental injection-level dependence of a-Si:H/c-Si interface recombination. It is allowing us thus to determine the respective contribution of interface defect reduction and field effect passivation to

interface recombination, and this on a large set of a-Si:H/c-Si configurations (intrinsic, lightly doped and doped of both doping types).

Final silicon heterojunction solar cells consist of an *i*/*p* a-Si:H layer stack grown on one side of a c-Si wafer and an *i*/*n* a-Si:H layer stack grown on its other side – plus an additionnal contact deposition. These cell's open-circuit voltages are already well predicted by the symmetrical surface passivation of the same c-Si wafer with single layers of intrinsic (*i*) a-Si:H. While *i*/*n* a-Si:H layer stacks are able to add field effect passivation to the low interface defect densities achieved with *i* a-Si:H passivation, *i*/*p*-stacks induce hardly any field effect passivation, while maintaining a medium defect density. Thus, at medium injection-levels, as corresponding to the maximum power point, the interface recombination resulting from merged front and back c-Si passivation is not yet sufficiently reduced. By tuning the injection-level dependence of the cells interface recombination such as to achieve simultaneously high lifetimes at all injection-levels we will be able to get rid off the trade-off between good open-circuit voltage V_{OC} (higher injection level) and high fill factors *FF* (medium injection-level). Up to now we were able to achieve in a short time on one hand a high-V_{OC} cell with V_{OC} = 705mV – but *FF* = 78% – and a high-*FF* cell with *FF* = 82% – but V_{OC} = 680mV.

An implementation of our simple a-Si:H/c-Si interface recombination model in a numerical simulation tool for solar cells could for example link these observed trade-offs between V_{OC} and FF to the injection-level dependence of interface recombination. However, our model should be extended to predict collection through the a-Si:H/c-Si interface: it should be completed with a transport model taking into account band-offsets to model extended states conduction and a-Si:H band tail states to model localized state conduction.

Acknowledgments

This work is supported by the Swiss National Foundation (FN-200021-107469).

References

[1] M.J. Kerr and A. Cuevas, Very low bulk and surface recombination in oxidized silicon wafers, *Semicond. Sci. Technol.*, **17**, 35-38 (2002).

[2] J. Schmidt and A.G. Aberle, Carrier recombination at silicon-silicon nitride interfaces fabricated by plasma-enhanced chemical vapor deposition, *J. Appl. Phys.*, **85**, 3626-3633 (1999).

[3] S.M. Sze, *Semiconductor devices: Physics and technology – 2nd edition*, J. Wiley & Sons, USA, 2002.

[4] A.G. Aberle, *Crystalline Silicon Solar Cells: Advanced Surface Passivation and Analysis*, Centre for Photovoltaic Engineering, University of New South Wales, Sydney, Australia, 1999.

[5] J. Hubin, A.V. Shah and E. Vallat-Sauvain, Effects of dangling bonds on the recombination function in amorphous semiconductors, *Philos. Mag. Lett.*, **66**, 115-125 (1992).

[6] R.A. Sinton and A. Cuevas, Contactless determination of current-voltage characteristics and minority-carrier lifetimes in semiconductors from quasi-steady-state photoconductance data, *Appl. Phys. Lett.*, **69**, 2510-2512 (1996).

[7] R.A. Sinton and A. Cuevas, "A Quasi-Steady-State Open-Circuit Voltage Method for Solar Cell Characterization", Proceedings of the 16th European Photovoltaic Solar Energy Conference (Glasgow, Scotland, may 2000), pp. 1152-1155, WIP, München (2000).